

**Assessment of simplified methods for quantification of  $^{18}\text{F}$ -FDHT uptake in patients with metastatic castration-resistant prostate cancer**

**Gerbrand M. Kramer<sup>1</sup>, Maqsood Yaqub<sup>1</sup>, Herbert A. Vargas<sup>2</sup>, Robert C. Schuit<sup>1</sup>, Albert D. Windhorst<sup>1</sup>, Alfonsus J.M. van den Eertwegh<sup>3</sup>, Astrid A.M. van der Veldt<sup>4,5</sup>, Andries M. Bergman<sup>4</sup>, Eva M. Burnazi<sup>2</sup>, Jason S. Lewis<sup>2,6</sup>, Sua Chua<sup>7</sup>, Kevin D. Staton<sup>2</sup>, Brad J. Beattie<sup>8</sup>, John L. Humm<sup>8</sup>, Ian D. Davis<sup>9</sup>, Andrew J. Weickhardt<sup>10</sup>, Andrew M. Scott<sup>10,11</sup>, Michael J. Morris<sup>12, 13</sup>, Otto S. Hoekstra<sup>1</sup>, Adriaan A. Lammertsma<sup>1</sup>**

*<sup>1</sup>Department of Radiology & Nuclear Medicine, Amsterdam UMC, Vrije Universiteit Amsterdam, Amsterdam, The Netherlands; <sup>2</sup>Department of Radiology, Memorial Sloan Kettering Cancer Center, New York, NY USA; <sup>3</sup>Department of Medical Oncology, Amsterdam UMC, Vrije Universiteit Amsterdam, Amsterdam, The Netherlands; <sup>4</sup>Department of Medical Oncology, Netherlands Cancer Institute, Amsterdam, the Netherlands; <sup>5</sup>Departments of Medical Oncology, Radiology & Nuclear Medicine, Erasmus Medical Center, Rotterdam, The Netherlands; <sup>6</sup>Department of Radiology, Weill Cornell Medicine, New York, NY USA; <sup>7</sup>Department of Nuclear Medicine, Royal Marsden NHS Foundation Trust, Sutton, UK; <sup>8</sup>Department of Medical Physics, Memorial Sloan Kettering Cancer Center, New York, NY USA; <sup>9</sup>Monash University and Eastern Health, Eastern Health Clinical School, Box Hill, Australia; <sup>10</sup>Department of Medical Oncology, Olivia Newton-John Cancer Research Institute, Austin Hospital, Melbourne, VIC, Australia; <sup>11</sup>Department of Molecular Imaging and Therapy, The University of Melbourne, Heidelberg, VIC Australia; <sup>12</sup>Department of Medicine, Memorial Sloan Kettering Cancer Center, New York, NY USA; <sup>13</sup>Department of Medicine, Weill Cornell Medicine, New York, NY USA.*

Word count: 5332

*Corresponding author:*

G.M. Kramer, M.D.

Department of Radiology & Nuclear Medicine

Amsterdam UMC, Vrije Universiteit Amsterdam

P.O. Box 7057, 1007 MB Amsterdam, the Netherlands

Tel: +31-20-4441532

E-mail: [ge.kramer@vumc.nl](mailto:ge.kramer@vumc.nl)

Short title: Simplified methods for FDHT quantitation

## **ABSTRACT**

### **OBJECTIVES:**

<sup>18</sup>F-fluorodihydrotestosterone (<sup>18</sup>F-FDHT) PET/CT potentially provides a non-invasive method for assessment of androgen receptor expression in patients with metastatic castration-resistant prostate cancer (mCRPC). The objective of this study was to assess simplified methods for quantifying <sup>18</sup>F-FDHT uptake in mCRPC patients and to assess effects of tumour perfusion on these <sup>18</sup>F-FDHT uptake metrics.

### **METHODS:**

Seventeen mCRPC patients were included in this prospective observational multicentre study. Test and retest 30 minute dynamic <sup>18</sup>F-FDHT PET/CT scans with venous blood sampling were performed in 14 patients. In addition, arterial blood sampling and dynamic <sup>15</sup>O-H<sub>2</sub>O scans were obtained in a subset of six patients. Several simplified methods were assessed: Patlak plots, standardized uptake values normalized to bodyweight (SUV<sub>BW</sub>) or lean body mass (SUV<sub>LBM</sub>), SUV normalized to whole blood (SUV<sub>WB</sub>) or parent plasma activity concentration (SUV<sub>PP</sub>), SUV normalized to the area under the parent plasma (SUV<sub>AUC,PP</sub>) or whole blood input curve (SUV<sub>AUC,WB</sub>), and SUV<sub>BW</sub> corrected for sex hormone-binding globulin (SHBG) levels (SUV<sub>SHBG</sub>). Results were correlated with parameters derived from full pharmacokinetic <sup>18</sup>F-FDHT and <sup>15</sup>O-H<sub>2</sub>O. Finally, repeatability of individual quantitative uptake metrics was assessed.

### **RESULTS:**

Eighty seven <sup>18</sup>F-FDHT avid lesions were evaluated. <sup>18</sup>F-FDHT uptake was best described by an irreversible 2-tissue compartment model. Replacing the continuous metabolite corrected arterial plasma input function with an image derived input function (IDIF) in combination with venous sample data provided similar K<sub>i</sub> results (R<sup>2</sup>=0.98). Patlak K<sub>i</sub> and SUV<sub>AUC,PP</sub> showed excellent correlation (R<sup>2</sup>>0.9). SUV<sub>BW</sub> showed a moderate correlation to K<sub>i</sub> (R<sup>2</sup>=0.70, presumably due to fast FDHT metabolism. When calculating SUV<sub>SHBG</sub>,

correlation to  $K_i$  improved ( $R^2=0.88$ ). Repeatability of full kinetic modelling parameters was inferior to that of simplified methods (repeatability coefficients  $>36\%$  vs.  $<28\%$ , respectively).  $^{18}\text{F}$ -FDHT uptake showed minimal blood flow dependency.

#### **CONCLUSION:**

$^{18}\text{F}$ -FDHT kinetics in mCRPC patients are best described by an irreversible 2-tissue compartment model with blood volume parameter.  $\text{SUV}_{\text{AUC,PP}}$  showed a near perfect correlation with the irreversible 2-tissue compartment model analysis and can be used for accurate quantification of  $^{18}\text{F}$ -FDHT uptake in whole-body PET/CT scans. In addition,  $\text{SUV}_{\text{SHBG}}$  could potentially be used as an even simpler method to quantify  $^{18}\text{F}$ -FDHT uptake when less complex scanning protocols and accuracy are required.

Key words: FDHT, PET/CT, prostate cancer, quantification

## INTRODUCTION

Prostate cancer is the most frequently diagnosed form of cancer in developed parts of the world and the second most common cause of cancer related mortality in US males leading to about 29.000 annual deaths (1,2). The androgen receptor (AR) plays a central role in both early and later stages of prostate cancer, including in metastatic castration-resistant prostate cancer (mCRPC). For mCRPC several mechanisms of AR-signalling persistence have been proposed, including persisting androgen production, AR overexpression, AR-splice variation and AR transcription via alternative signalling pathways (3). Several agents have been developed that specifically target the AR (e.g. enzalutamide and abiraterone). In mCRPC patients, both with and without prior treatment with docetaxel, these drugs have shown improved survival and quality of life (4,5).

<sup>18</sup>F-fluorodihydrotestosterone (<sup>18</sup>F-FDHT) is a positron emitting tracer that provides a means to in vivo image the AR in mCRPC patients (6,7). Therefore, <sup>18</sup>F-FDHT positron emission tomography/computed tomography (PET/CT) could potentially be used as an imaging biomarker to evaluate AR status and pharmacological targeting on a lesion-by-lesion level. This is of particular significance since mechanisms of persistent AR-signalling can differ between metastatic lesions. (8,9). In mCRPC, direct assessment of AR using <sup>18</sup>F-FDHT could aid AR-targeted drug development, and more personalized treatment planning, thereby potentially preventing unnecessary toxicities and costs.

Accurate quantification is required for objective evaluation of <sup>18</sup>F-FDHT uptake in mCRPC lesions. The gold standard for quantification of tracer uptake is pharmacokinetic modelling using non-linear regression (NLR) in combination with a metabolite corrected arterial plasma input function (10). At present, NLR is incompatible with whole body acquisitions typically required in patients with metastatic disease. Development of total body PET scanners may overcome this problem. Moreover, because of its complexity, this method it is not well suited for daily clinical practice or large multicentre studies where

simpler methods such as standardized uptake values (SUV) are preferred. Although pharmacokinetic assessment of  $^{18}\text{F}$ -FDHT uptake has been performed by Beattie et al. (6), a population based input function was used rather than individually measured arterial input functions. This could have confounded results due to inter-subject differences in individual arterial input functions.

Full understanding of  $^{18}\text{F}$ -FDHT kinetics is essential for developing simplified methods to quantify  $^{18}\text{F}$ -FDHT uptake in clinical practice. Therefore, the objectives of this study were: 1. To identify the optimal pharmacokinetic model for quantifying  $^{18}\text{F}$ -FDHT kinetics in mCRPC patients using individually measured arterial input functions; 2. To comprehensively investigate whether simplified methods can be used for accurate quantification of  $^{18}\text{F}$ -FDHT uptake; 3. To measure repeatability of  $^{18}\text{F}$ -FDHT uptake metrics; and 4. To assess potentially confounding effects of perfusion on these simplified  $^{18}\text{F}$ -FDHT uptake metrics.

## **METHODS**

### **Patients**

Between July 2014 and October 2017, 17 histologically proven mCRPC patients were included at the VU University Medical Center, the Netherlands and Memorial Sloan Kettering Cancer Center, United States. Fifteen patients were also included in a previous publication assessing the repeatability of whole body quantitative  $^{18}\text{F}$ -FDHT uptake metrics (11). Patient eligibility criteria were: castration-resistant prostate cancer (castrate levels of serum testosterone  $<1.7 \text{ nmol}\cdot\text{L}^{-1}$  [ $50\text{ng}\cdot\text{dL}^{-1}$ ]); no treatment with enzalutamide or other anti-androgens within 4 weeks prior to study entry; no other malignancies; at least one lesion within the field of view positioned over the ascending aorta; and progressive disease based on any of the following: (a) a rise in serum PSA through 3 consecutive measurements; (b) RECIST

1.1 imaging evidence of progressive disease and/or (c) bone scan showing at least two new metastatic lesions not attributable to the flare phenomenon. Patients without orchiectomy remained on androgen depletion therapy with a gonadotropin-releasing hormone analogue or inhibitor during the study. This study was approved by the institutional review boards of both centres and all participants gave written informed consent prior to study enrolment. This trial is registered at [clinicaltrials.gov](http://clinicaltrials.gov) (NCT00588185, this number applies only to Memorial Sloan Kettering, the only United States based site).

### **PET Imaging**

$^{18}\text{F}$ -FDHT PET/CT scans were obtained using a GE 690, a GE710 (General Electric, Fairfield, USA) or a Philips Gemini TF 64 (Philips Healthcare, Eindhoven, The Netherlands) PET/CT scanner. All participants underwent double baseline  $^{18}\text{F}$ -FDHT scans on two consecutive days. Sex hormone-binding globulin levels were determined at the day of the first scan. First a low-dose CT (120-140 kV) was performed during tidal breathing, directly followed by a 30 min dynamic  $^{18}\text{F}$ -FDHT PET scan over the thorax starting simultaneously with intravenous  $^{18}\text{F}$ -FDHT administration. The tracer was either administered manually at a rate of  $0.5\text{mL}\cdot\text{s}^{-1}$  during 3-10 s followed by  $>40\text{mL}$  saline in 30-60 s, or using an automated injector (Medrad, Warrendale, United States) flushed with 40 mL of saline (5 mL at  $0.8\text{mL}\cdot\text{s}^{-1}$  followed by 35 mL at  $2\text{mL}\cdot\text{s}^{-1}$ ). After injection residual activity in syringe and lines was measured. Dynamic  $^{18}\text{F}$ -FDHT data were reconstructed into 19 frames (6x5, 3x10, 4x60, 2x150 and 4x300 s) and corrected for detector inhomogeneity, dead-time, decay, scatter, random coincidences and photon attenuation, the latter using the low-dose CT scan. An ordered subset expectation maximization algorithm was used for reconstruction of the images. In addition, during the dynamic  $^{18}\text{F}$ -FDHT scan, three manual venous samples were drawn from a separate intravenous cannula at 5, 10 and 30 min post-injection (12). For all samples whole blood and plasma activity concentrations were measured, as well as parent and metabolite fractions of  $^{18}\text{F}$ -FDHT. Radiometabolite analysis was performed using high-

performance liquid chromatography at the VU University Medical Center. At Memorial Sloan Kettering Cancer Center a simplified method was used. High-performance liquid chromatography was only performed for the first and last blood sample, for the other samples an extraction technique was used and, combined with the high-performance liquid chromatography data, the parent fraction was determined. Details on the radiometabolite analysis method used can be found in Beattie et al.(6).

Furthermore, a subset of patients underwent continuous arterial sampling at  $5 \text{ mL}\cdot\text{min}^{-1}$  during the first 5 min and at  $2.5 \text{ mL}\cdot\text{min}^{-1}$  thereafter until the end of the dynamic  $^{18}\text{F}$ -FDHT scan. Continuous sampling was interrupted at 5, 10, 15, 20, 30, 45 min post-injection to obtain manual arterial samples for determination of whole blood activity concentrations, plasma activity concentrations, together with parent and metabolite fractions. These patients also underwent a dynamic 10 min  $^{15}\text{O}$ -H<sub>2</sub>O scan prior to the first dynamic  $^{18}\text{F}$ -FDHT scan. Injection of  $^{15}\text{O}$ -H<sub>2</sub>O (370 MBq) was performed using an automated injector (Medrad), and flushed using 40 mL of saline (5 mL at  $0.8 \text{ mL}\cdot\text{s}^{-1}$  followed by 35 mL at  $2 \text{ mL}\cdot\text{s}^{-1}$ ). After the  $^{15}\text{O}$ -H<sub>2</sub>O PET scan a low-dose CT (120 Kv) was acquired for attenuation correction. The dynamic  $^{15}\text{O}$ -H<sub>2</sub>O data were reconstructed into 26 frames (1x10, 8x5, 4x10, 2x15, 3x20, 2x30 and 6x60 s) using the same correction and reconstruction methods as for the dynamic  $^{18}\text{F}$ -FDHT scans.

## Data Analysis

All  $^{18}\text{F}$ -FDHT avid tumours were delineated on an averaged image generated from the last 15 min of the dynamic  $^{18}\text{F}$ -FDHT scan, using a 50% isocontour of  $\text{SUV}_{\text{peak}}$  (sphere of 1.2 cm diameter, positioned to maximize its mean value) corrected for local background to obtain volumes of interest (VOIs)(Fig. 1) (12). Time-activity curves were produced by projecting tumour VOIs on the dynamic  $^{18}\text{F}$ -FDHT and, where applicable,  $^{15}\text{O}$ -H<sub>2</sub>O scans. In addition, image derived input functions (IDIFs) were obtained from  $^{18}\text{F}$ -FDHT and  $^{15}\text{O}$ -H<sub>2</sub>O scans by placing a 2 x 2 voxel VOI centrally on the ascending aorta in 5 consecutive planes

using an early frame in which the blood pool was clearly visible. Corresponding time-activity curves were generated by projecting these VOIs onto  $^{18}\text{F}$ -FDHT and  $^{15}\text{O}$ -H<sub>2</sub>O scans.

Both arterially sampled input curves and IDIFs (600-2000 s) were calibrated using the manual arterial blood samples. Subsequently, these calibrated input curves were corrected for plasma-to-whole blood ratios and metabolites to generate parent plasma input functions using a multi exponential fit and Hill fit (13), respectively. For IDIFs this procedure was repeated using the manual venous blood samples (IDIF<sub>venous</sub>).

Pharmacokinetic modelling was performed using in-house developed software in MATLAB (MathWorks Inc, Natick, MA).  $^{15}\text{O}$ -H<sub>2</sub>O scans were analysed using the standard single tissue reversible arterial input model with additional blood volume fraction parameter and the kinetic rate constant  $K_1$  was used as outcome parameter (14).  $^{18}\text{F}$ -FDHT data were analysed using one-tissue, and both irreversible and reversible two-tissue compartment models, all with an additional blood volume fraction parameter consisting of whole blood activity (10,15). Net influx rate ( $K_i$ ) and volume of distribution ( $V_T$ ) were calculated from fitted kinetic rate constants: 2-tissue irreversible  $K_i = K_1 \cdot k_3 / (k_2 + k_3)$ , 2-tissue reversible two compartment  $V_T = K_1 / k_2 \cdot (1 + k_3 / k_4)$  and 2-tissue reversible one compartment  $V_T = K_1 / k_2$ . The optimal fit was obtained from the best among 20 constrained fits each initialized with randomly chosen starting parameters. The constraints of the pharmacokinetic parameters were:  $K_1$  (0-2);  $k_2$  (0-100);  $k_3$  (0.025-100);  $k_3/k_4$  (0-100). Furthermore, several simplified uptake metrics were derived from the  $^{18}\text{F}$ -FDHT data: (A) Patlak  $K_i$  ( $t^*=5$  min post-injection); (B) SUV normalized to both bodyweight (SUV<sub>BW</sub>) and lean body mass (SUV<sub>LBM</sub>); (C) SUV normalized to the whole blood activity concentration (SUV<sub>WB</sub>); (D) SUV normalized to the parent plasma concentration (SUV<sub>PP</sub>); (E) SUV normalized to the area under the whole blood input curve (SUV<sub>AUC,WB</sub>); (F) SUV normalized to the area under the parent plasma input curve

( $SUV_{AUC,PP}$ ); and (G)  $SUV_{BW}$  corrected for serum SHBG levels ( $SUV_{SHBG}=SUV_{BW}/\text{serum SHBG}$ ). All SUV uptake intervals were set to 20-30 minutes post-injection (6).

## **Statistical Analysis**

Normality of the data was assessed visually using a quantile-quantile plot and histogram analysis. The Akaike criterion was used to select the preferred model for describing kinetics of  $^{18}\text{F}$ -FDHT in patients undergoing arterial blood sampling (16). Pharmacokinetic outcome measures calculated using the metabolite corrected arterial plasma input functions were correlated against pharmacokinetic outcome measures obtained using IDIFs and perfusion metrics. Performance of simplified uptake metrics was assessed in a head-to-head comparison with pharmacokinetic outcome measures from NLR. These analyses were performed using linear regression analysis, intraclass correlation coefficients (ICCs) and Bland-Altman plots. In addition, where applicable, repeatability of all outcome measures was assessed using repeatability coefficients (RCs) calculated as  $1.96 \times \text{SD}$  of the relative differences per lesion. Levene's test was performed to assess differences in RCs between outcome measures. Differences were deemed significant if  $p < 0.05$ . All statistical analyses were performed using SPSS 22.0 (SPSS, Chicago, IL, USA).

## **RESULTS**

### **Pharmacokinetic Modelling**

Fourteen patients, with a total of 87 lesions, were enrolled (Table 1). Three patients were excluded due to incomplete or missing blood sample data. Overall, plasma-to-blood ratios remained stable over time, however  $^{18}\text{F}$ -FDHT underwent fast metabolism and about 90% was metabolized at 30 minutes post-injection (Supplemental fig. 1).

Continuous arterial blood sampling in combination with manual arterial sampling was performed in a subset of six patients with 44  $^{18}\text{F}$ -FDHT avid lesions. Based on the Akaike criterion tumour time-activity curves were best described by an irreversible 2-tissue model in 34%, a reversible 2-tissue two compartment model in 27% and a reversible 2-tissue one compartment model in 39% of the lesions. In 52% of the lesions, the difference in Akaike criterion between the pharmacokinetic models was <15 points). All individual  $K_i$  values were within normal range, whilst  $V_T$  values suffered from outliers in 36% of the cases for the reversible 2-tissue two-compartment model and 7% for the reversible 2-tissue one compartment model. Therefore, the irreversible 2-tissue model was used for further evaluation of  $^{18}\text{F}$ -FDHT (Fig. 2). Replacing the continuous arterial plasma input function with  $\text{IDIF}_{\text{venous}}$  provided similar  $K_i$  results ( $R^2=0.98$ ;  $\text{ICC}=0.99$ ) (Fig. 3). Results of full kinetic modelling and simplified methods are shown in Supplemental table 1.

Considering the strong correlation with  $K_i$  obtained using continuous arterial sampling,  $K_i$  obtained using  $\text{IDIF}_{\text{venous}}$  was used for validation of simplified methods. Fourteen lesions were excluded due to unrealistically high  $k_2$  values and SDs ( $k_2 > 1$ ). An excellent correlation was found between Patlak  $K_i$  and NLR derived  $K_i$  ( $R^2=0.99$ ;  $\text{ICC}=0.99$ ). This was also the case for  $\text{SUV}_{\text{AUC,PP}}$ , but performances of more simplified methods were poorer (Fig. 4, Table 2 and Supplemental Fig. 2). No significant differences were found in accuracy between  $\text{SUV}_{\text{BW}}$  and  $\text{SUV}_{\text{LBM}}$ . When  $\text{SUV}_{\text{BW}}$  was corrected for serum SHBG levels ( $\text{SUV}_{\text{SHBG}}$ ) overall correlation with full kinetic modelling improved ( $R^2=0.88$ ). A direct comparison of serum SHBG to the rate of  $^{18}\text{F}$ -FDHT metabolism, calculated as the AUC of the parent plasma input function, did not show a strong relationship ( $R^2=0.32$ ). All simplified methods reached equilibrium at 30 min after injection, except for  $\text{SUV}_{\text{pp}}$ , which still showed a steep increase.

## Repeatability

Repeated baseline scans were available in 10 patients with a total of 80 lesions. Median plasma-to-blood and parent plasma fractions at 30 min were not significantly different between test and retest scans ( $p>0.7$ ) (Supplemental fig. 1). Correlation between test and retest scans was strong for all quantitative metrics ( $R^2=0.86-0.93$ ;  $ICC>0.95$ ). The repeatability coefficient of NLR derived  $K_i$  using IDIF corrected with venous sample data was 36% (Fig. 5). Except for  $SUV_{pp}$ , quantitatively assessing  $^{18}F$ -FDHT uptake using simplified methods reduced variability ( $RC=23-31\%$ ) (Table 3, Fig. 5 and Supplemental table 2 and Supplemental Fig. 3). Repeatability of all uptake metrics showed a trend towards dependency on lesion size. In addition, for  $SUV_{pp}$  and  $SUV_{BW}$  repeatability appears to improve for higher SUV values.

## Perfusion

Thirty-five lesion (30 bone and 5 lymph node metastases) were available for assessing the correlation between perfusion and quantitative  $^{18}F$ -FDHT uptake metrics.  $K_i$  values obtained using the irreversible 2-tissue compartment model with  $IDIF_{venous}$  as well as  $^{18}F$ -FDHT plasma extraction showed minimal blood flow dependency ( $R_2= 0.23$  and  $0.30$  respectively)(Fig. 6). In addition, effects of perfusion on the discrepancy between SUV and NLR based  $K_i$  for  $^{18}F$ -FDHT was assessed by plotting the ratio of  $SUV/K_i$  against  $^{15}O$ - $H_2O$  derived  $K_1$ . This plot showed no correlation with blood flow for any of the SUVs ( $R^2\leq 0.01$ )(Supplemental Fig. 4).

## DISCUSSION

This multicentre study addressed the important clinical question whether simplified uptake metrics can be used to measure  $^{18}F$ -FDHT uptake in mCRPC both accurately and precisely. An irreversible 2-tissue model with blood volume fraction parameter was preferred for characterizing tumour  $^{18}F$ -FDHT

kinetics. This is congruent with previous findings from Beattie et al. (6), where both irreversible 1- and 2-tissue models provided the best fits in the majority of the cases. The preference for the irreversible 2-tissue model is also logical from a physiological perspective. In this model  $K_1$  presumably represents influx of FDHT into the cell. After influx,  $^{18}\text{F}$ -FDHT binds to AR (the presumptive second compartment described by  $k_3$ ) and is then transported into the nucleus. It could therefore be argued that  $k_3$  is a more appropriate measure for assessment of AR expression, as it describes the binding of  $^{18}\text{F}$ -FDHT to the AR rather than uptake in the prostate cancer cell. Finally,  $k_2$  represents efflux of unbound  $^{18}\text{F}$ -FDHT out of the prostate cancer cell. It has been suggested that  $^{18}\text{F}$ -FDHT binding might be reversible at later time-points (6,17) and that slow reversibility may potentially develop > 1 hour after injection of  $^{18}\text{F}$ -FDHT.

Pharmacokinetic measures obtained using an  $\text{IDIF}_{\text{venous}}$  correlated well with those obtained using a continuous arterial plasma input function. There was a slight negative bias (5%), which could be due to temporal differences between the two input functions. In addition, no significant differences were found between plasma-to-blood ratios and parent fractions of venous and arterial blood samples. This indicates that arterial blood sampling is not required in case of  $^{18}\text{F}$ -FDHT quantification. There was an almost perfect correlation between  $\text{SUV}_{\text{AUC,PP}}$  and  $K_i$  derived from pharmacokinetic analysis, eliminating the need for dynamic scanning. Nevertheless,  $\text{SUV}_{\text{AUC,PP}}$  still requires an additional 30 min static PET scan over the chest together with metabolite analysis of a number of venous blood samples. This enables accurate quantification of lesions outside of the thorax, although metabolite analysis may limit its feasibility in multicentre studies and daily clinical practice. Automation of  $^{18}\text{F}$ -FDHT metabolite analysis could potentially overcome these limitations.

As an alternative, SUV only requires a single static whole body scan without any blood sampling. However, in line with Beattie et al. (6), SUV only showed a moderate correlation with pharmacokinetic outcome measures. This poorer correlation was primarily caused by one subject with very extensive

disease (>40 lesions) and relatively low SHBG levels. In blood, the majority of dihydrotestosterone is bound to proteins (mainly SHBG). Yet, as postulated in the free hormone hypothesis, only free circulating dihydrotestosterone is able to bind to the AR (18,19). In a murine prostate cancer model, Larimer et al. (17) showed that differences in tissue-to-blood ratios between free circulating and SHBG bound  $^{18}\text{F}$ -FDHT were only small at 1 hour post-injection. However, blood pool activity was significantly higher in SHBG bound  $^{18}\text{F}$ -FDHT at 1 hour post-injection indicating a lower metabolic rate compared with freely circulating FDHT and an increased tumour uptake as tissue-to-blood ratios are comparable. Normalizing SUV for interpatient differences in serum SHBG levels significantly improved correlation with NLR derived  $K_i$ . Nevertheless the rate of  $^{18}\text{F}$ -FDHT metabolism levels only showed a moderate correlation with serum SHBG (data not shown). Determining serum SHBG just prior to the  $^{18}\text{F}$ -FDHT scan could potentially be used as a surrogate for more cumbersome parent plasma fraction measurements. SHBG measurements are widely available, which would facilitate application in clinical practice or larger trials. However, further research is needed before SHBG can be used as a surrogate for metabolite analysis.

Changes in tumour perfusion due to physiological variability or treatment could potentially affect tracer uptake when it is perfusion limited. For  $K_i$  a poor correlation was found with  $^{15}\text{O}$ - $\text{H}_2\text{O}$  derived  $K_1$  and therefore  $K_i$  does not seem to depend on tumour perfusion. Even though  $^{18}\text{F}$ -FDHT is rapidly cleared from blood plasma,  $k_3$  values were relatively small compared with  $k_2$  values, thereby limiting the effects of perfusion on  $^{18}\text{F}$ -FDHT uptake.  $\text{SUV}_{\text{BW}}$  and  $\text{SUV}_{\text{SHBG}}$  showed somewhat stronger and weaker correlations with  $^{15}\text{O}$ - $\text{H}_2\text{O}$   $K_1$ , respectively. However, discrepancies of  $\text{SUV}_{\text{BW}}$  and  $\text{SUV}_{\text{SHBG}}$  with  $^{18}\text{F}$ -FDHT  $K_i$  were not due to differences in perfusion.

Before quantitative uptake metrics can be used in a response assessment setting, repeatability should be known. A highly accurate parameter cannot be used for response measurements if precision is poor. RCs found for SUV in the present study were similar to those found in a previous study for whole

body quantitative  $^{18}\text{F}$ -FDHT uptake metrics and in line with those of other F-18 labelled tracers (11,20,21). Repeatability of full kinetic modelling parameters obtained using an irreversible 2-tissue compartment model showed, higher variability than those of more simplified methods, with exception of  $\text{SUV}_{\text{PP}}$ . NLR analysis is known to be more vulnerable to noise, but it can account for changes in pharmacokinetics after therapy. Pharmacokinetic assessment of quantitative tracer uptake should therefore be performed before simplified methods can be used in a response evaluation setting. In the present study no RCs could be calculated for  $\text{SUV}_{\text{SHBG}}$  as SHBG levels were only determined prior to the first  $^{18}\text{F}$ -FDHT scan. Nevertheless, previous studies found small fluctuations in SHBG levels within two consecutive days and therefore the influence of SHBG on repeatability is expected to be minimal (22).

In the present study, validation of simplified  $^{18}\text{F}$ -FDHT uptake metrics was performed in mCRPC patients. This is an essential step in the development of  $^{18}\text{F}$ -FDHT as an imaging biomarker for prognosis, response, and AR-targeted drug development by direct evaluation of AR status on a lesion-by-lesion level.  $\text{SUV}_{\text{AUC,PP}}$  and, to a lesser extent,  $\text{SUV}_{\text{SHBG}}$  seemed to be the preferred simplified methods for quantification of  $^{18}\text{F}$ -FDHT uptake.  $\text{SUV}_{\text{SHBG}}$  is more attractive in clinical practice and for larger multicentre trials, as it only requires a single whole body  $^{18}\text{F}$ -FDHT scan and SHBG blood sample. However, exact repeatability coefficients of this uptake measure still need to be determined. The correlation of  $\text{SUV}_{\text{AUC,PP}}$  with  $K_i$  derived from full pharmacokinetic analysis was much stronger than for  $\text{SUV}_{\text{SHBG}}$ , although at the cost of an additional early scan over the chest and metabolite analysis to obtain the parent plasma input function. This method is preferred when high accuracy is required. An additional advantage of including  $\text{SUV}_{\text{AUC,PP}}$  in an investigational setting is that more simplified methods can also be assessed.  $\text{SUV}_{\text{AUC,PP}}$  and  $\text{SUV}_{\text{SHBG}}$  can both be used for whole-body acquisitions, which is essential in mCRPC as most lesions are located outside of the thorax. As a next step in the development of  $^{18}\text{F}$ -FDHT PET/CT as an imaging biomarker the performance of these quantitative uptake metrics need to be assessed in biological and clinical validation studies.

The small amount of patients is an inherent limitation to pharmacokinetic modelling studies. High patient burden and costly procedures limit the amount of scans that can be acquired. Nevertheless we performed a multicentre study and double baseline scanning to maximize the reliability of the pharmacokinetic  $^{18}\text{F}$ -FDHT modelling. Unfortunately the majority of the scans were obtained from one centre, however a multicentre pharmacokinetic studies are exceptional and most are performed in monocentre setting.

## **CONCLUSION**

An irreversible two-tissue compartment model with blood volume parameter best described  $^{18}\text{F}$ -FDHT kinetics in mCRPC patients.  $\text{SUV}_{\text{AUC,PP}}$  correlated near perfectly with  $K_i$  obtained using full pharmacokinetic analysis and can be used for accurate quantification of  $^{18}\text{F}$ -FDHT uptake in whole-body PET/CT scans. Therefore,  $\text{SUV}_{\text{AUC,PP}}$  is recommend when high accuracy is required. In addition,  $\text{SUV}_{\text{SHBG}}$  also showed a strong correlation with  $K_i$  and could be considered when less accuracy is required.

## **DISCLOSURE**

This study was funded by a Movember Foundation Global Action Plan award. The Memorial Sloan Kettering Cancer Center is supported by NIH/NCI Cancer Center Support Grant P30 CA008748. IDD is supported by an Australian NHMRC Practitioner Fellowship (APP1102604). No potential conflicts of interest relevant to this article exist.

## REFERENCES:

1. Ferlay J, Soerjomataram I, Dikshit R, et al. Cancer incidence and mortality worldwide: sources, methods and major patterns in GLOBOCAN 2012. *Int J Cancer*. 2015;136:E359-386.
2. Siegel RL, Miller KD, Jemal A. Cancer statistics, 2018. *CA Cancer J Clin*. 2018;68:7-30.
3. Ferraldeschi R, Welti J, Luo J, Attard G, de Bono JS. Targeting the androgen receptor pathway in castration-resistant prostate cancer: progresses and prospects. *Oncogene*. 2015;34:1745-1757.
4. Scher HI, Fizazi K, Saad F, et al. Increased survival with enzalutamide in prostate cancer after chemotherapy. *N Engl J Med*. 2012;367:1187-1197.
5. Beer TM, Armstrong AJ, Rathkopf D, et al. Enzalutamide in men with chemotherapy-naive metastatic castration-resistant prostate cancer: extended analysis of the phase 3 PREVAIL study. *Eur Urol*. 2017;71:151-154.
6. Beattie BJ, Smith-Jones PM, Jhanwar YS, et al. Pharmacokinetic assessment of the uptake of 16beta-18F-fluoro-5alpha-dihydrotestosterone (FDHT) in prostate tumors as measured by PET. *J Nucl Med*. 2010;51:183-192.
7. Bonasera TA, O'Neil JP, Xu M, et al. Preclinical evaluation of fluorine-18-labeled androgen receptor ligands in baboons. *J Nucl Med*. 1996;37:1009-1015.
8. Larson SM, Morris M, Gunther I, et al. Tumor localization of 16beta-18F-fluoro-5alpha-dihydrotestosterone versus 18F-FDG in patients with progressive, metastatic prostate cancer. *J Nucl Med*. 2004;45:366-373.
9. Vargas HA, Wassberg C, Fox JJ, et al. Bone metastases in castration-resistant prostate cancer: associations between morphologic CT patterns, glycolytic activity, and androgen receptor expression on PET and overall survival. *Radiology*. 2014;271:220-229.
10. Gunn RN, Gunn SR, Cunningham VJ. Positron emission tomography compartmental models. *J Cereb Blood Flow Metab*. 2001;21:635-652.
11. Vargas HA, Kramer GM, Scott AM, et al. Reproducibility and repeatability of semiquantitative (18)F-fluorodihydrotestosterone uptake metrics in castration-resistant prostate cancer metastases: a prospective multicenter study. *J Nucl Med*. 2018;59:1516-1523.
12. Frings V, Yaqub M, Hoyng LL, et al. Assessment of simplified methods to measure 18F-FLT uptake changes in EGFR-mutated non-small cell lung cancer patients undergoing EGFR tyrosine kinase inhibitor treatment. *J Nucl Med*. 2014;55:1417-1423.
13. Gunn RN, Sargent PA, Bench CJ, et al. Tracer kinetic modeling of the 5-HT1A receptor ligand [carbonyl-11C]WAY-100635 for PET. *Neuroimage*. 1998;8:426-440.
14. van der Veldt AA, Hendrikse NH, Harms HJ, et al. Quantitative parametric perfusion images using 15O-labeled water and a clinical PET/CT scanner: test-retest variability in lung cancer. *J Nucl Med*. 2010;51:1684-1690.

15. Yaqub M, Boellaard R, Kropholler MA, Lammertsma AA. Optimization algorithms and weighting factors for analysis of dynamic PET studies. *Phys Med Biol.* 2006;51:4217-4232.
16. Akaike H. A new look at the statistical model identification. *IEEE Trans Automat Contr.* 1974;19:716-723.
17. Larimer BM, Dubois F, Bloch E, et al. Specific (18)F-FDHT accumulation in human prostate cancer xenograft murine models is facilitated by prebinding to sex hormone-binding globulin. *J Nucl Med.* 2018;59:1538-1543.
18. Swerdloff RS, Dudley RE, Page ST, Wang C, Salameh WA. Dihydrotestosterone: biochemistry, physiology, and clinical implications of elevated blood levels. *Endocr Rev.* 2017;38:220-254.
19. Selby C. Sex hormone binding globulin: origin, function and clinical significance. *Ann Clin Biochem.* 1990;27 ( Pt 6):532-541.
20. Kramer GM, Frings V, Hoetjes N, et al. Repeatability of quantitative whole-body 18F-FDG PET/CT uptake measures as function of uptake interval and lesion selection in non-small cell lung cancer patients. *J Nucl Med.* 2016;57:1343-1349.
21. Oprea-Lager DE, Kramer G, van de Ven PM, et al. Repeatability of quantitative 18F-fluoromethylcholine PET/CT studies in prostate cancer. *J Nucl Med.* 2016;57:721-727.
22. Brambilla DJ, Matsumoto AM, Araujo AB, McKinlay JB. The effect of diurnal variation on clinical measurement of serum testosterone and other sex hormone levels in men. *J Clin Endocrinol Metab.* 2009;94:907-913.

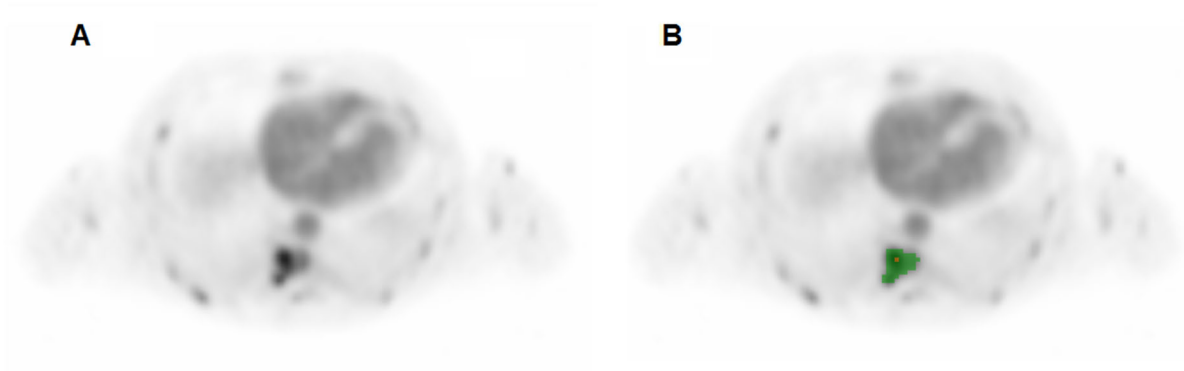


Figure 1: An example of an averaged image generated from the last 15 min of the dynamic  $^{18}\text{F}$ -FDHT scan (A). All tumours were delineated using a 50% isocontour of  $\text{SUV}_{\text{peak}}$  (sphere of 1.2 cm diameter, positioned to maximize its mean value) corrected for local background (B). The yellow voxel indicates the hottest voxel in the VOI.

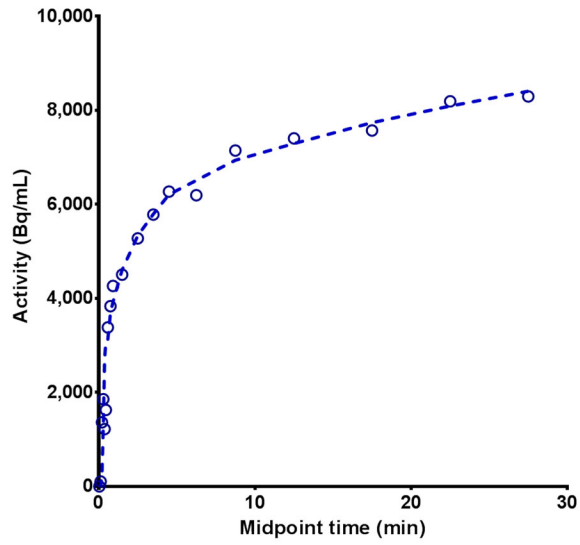


Figure 2: A typical example of a  $^{18}\text{F}$ -FDHT uptake in a metastatic prostate cancer lesions fitted using an irreversible 2-tissue model with blood volume fraction parameter.

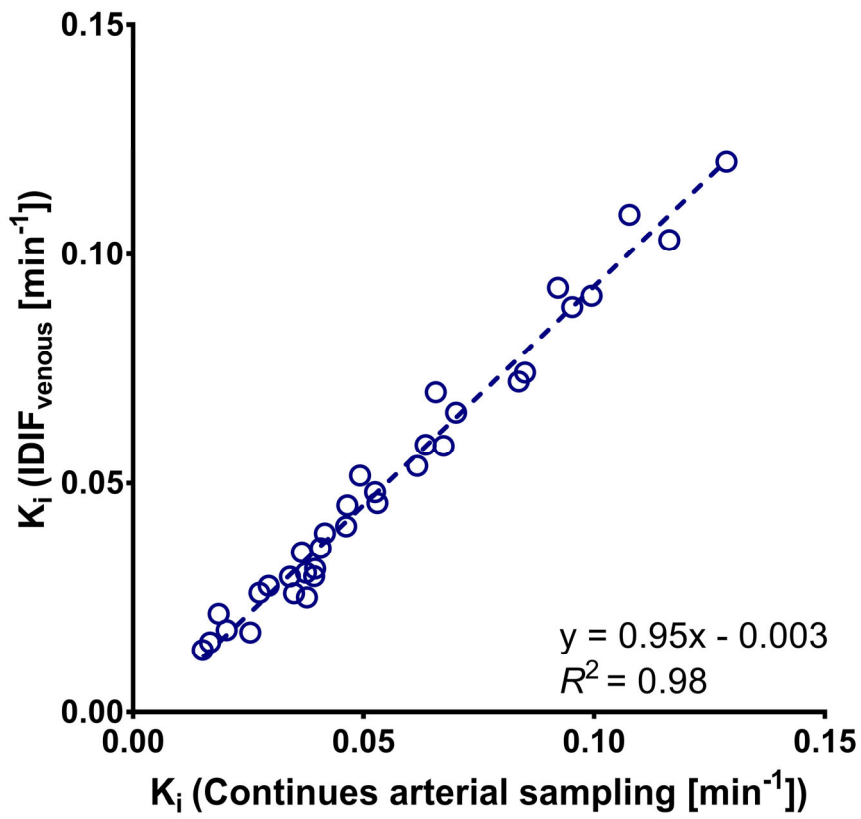


Figure 3: <sup>18</sup>F-FDHT  $K_i$  obtained using an image derived input function corrected using venous blood samples (IDIF<sub>venous</sub>) plotted against those obtained using continues arterial sampling (N=34).

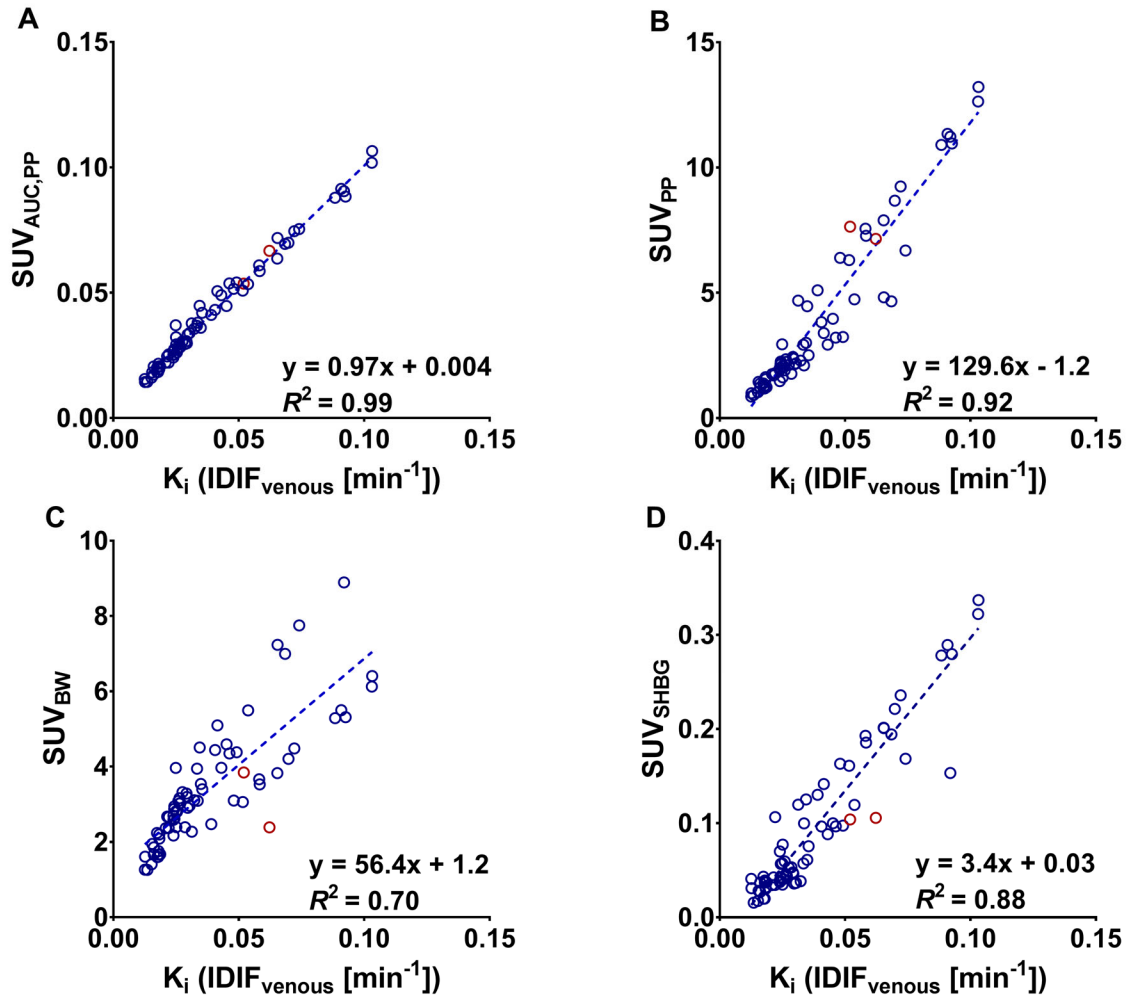


Figure 4: Scatterplots showing the correlation of  $^{18}\text{F}$ -FDHT  $SUV_{AUC,PP}$  (A),  $SUV_{PP}$  (B),  $SUV_{BW}$  (C) and  $SUV_{SHBG}$  (D) with  $K_i$  obtained using an image derived input function corrected for metabolites using venous blood samples (IDIF<sub>venous</sub>)(N=87). (Blue: Philips Gemini TF 64; Red: GE 690 or GE710).

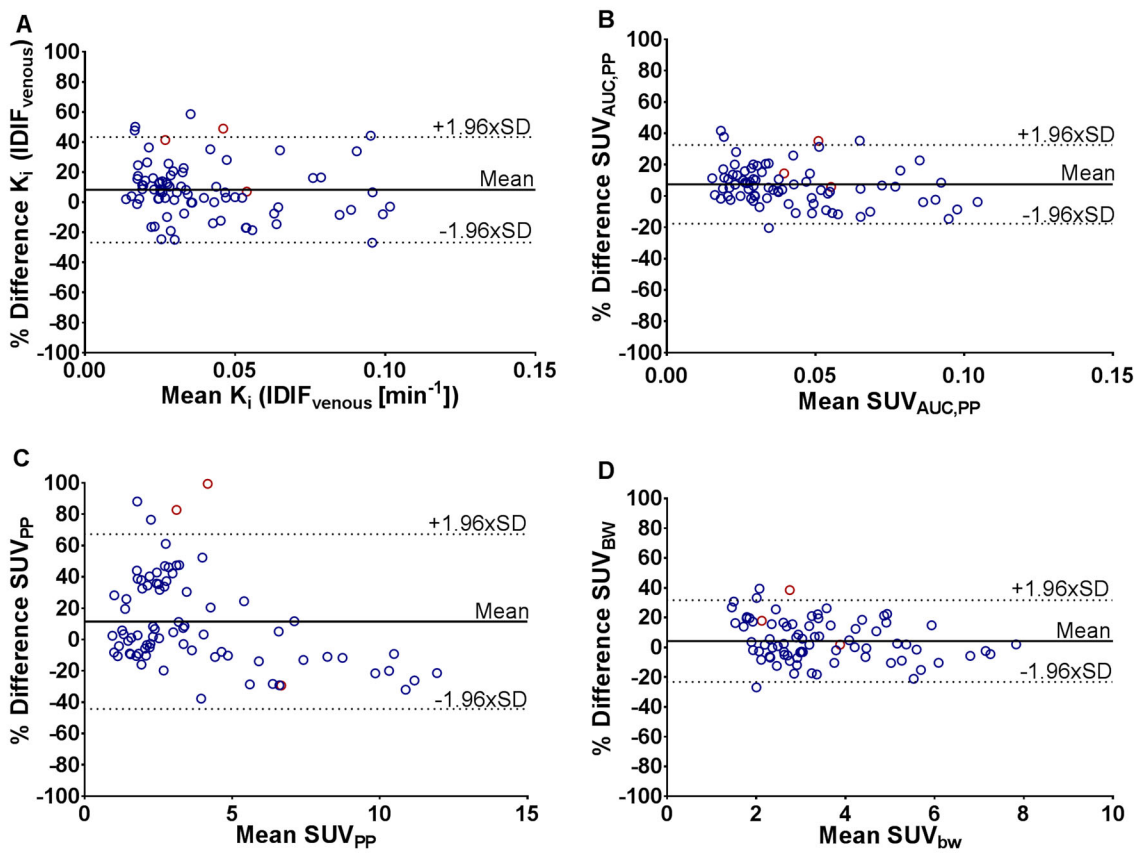


Figure 5: Bland-Altman plots showing the relative differences in  $^{18}\text{F}$ -FDHT uptake between test and retest  $K_i$  obtained using an image derived input function corrected using venous blood samples (A),  $\text{SUV}_{\text{AUC,PP}}$  (B),  $\text{SUV}_{\text{PP}}$  (C) and  $\text{SUV}_{\text{BW}}$  (D) (N=80). (Blue: Philips Gemini TF 64; Red: GE 690 or GE710).

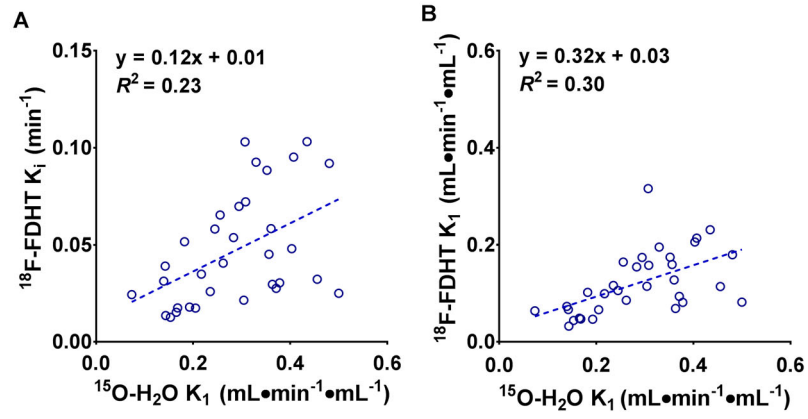


Figure 6: NLR based  $K_i$  (A) and  $K_1$  (B) using venous blood sampling and  $\text{SUV}_{\text{SHBG}}$  plotted against  $^{15}\text{O-H}_2\text{O}$  based  $K_1$ .

Table 1. Patient characteristics (n=14)

	Median (range)	n
Age (years)	69 (58-85)	
Length (cm)	180 (170-194)	
Weight (kg)	83 (65-125)	
Gleason Score	8 (5-10)	
PSA (ng/mL)	102.5 (0.5-1602)	
SHBG (nmol/L)	41 (19-81)	
Injected activity (MBq)		
- Test	197 (174-337)	
- Retest	196 (186-342)	
Residual dose (MBq)		
- Test	31.4 (18.2-55.7)	
- Retest	34.5 (6.1-53.5)	
Lesions (n)		
- Bone		75
- Lymph node		12
Location (n)		
- Thoracic vertebrae		36
- Ribs		24
- Sternum		8
- Scapulae		6
- Humerus		1
- Mediastinal lymphnodes		12
- Axillary lymphnodes		1
Scanner Type (n)		
- Philips Gemini TF 64		11
- GE 690 or GE710		3
Sampling (n)		
- Arterial		6
- Venous		14

Table 2: Correlation of simplified methods with  $K_i$  obtained using pharmacokinetic modelling

	Continues arterial sampling			IDIF <sub>venous</sub>		
	R <sup>2</sup>	Slope	Intercept	R <sup>2</sup>	Slope	Intercept
Patlak $K_i$	0.99	0.90	0.00	0.99	0.93	0.00
SUV <sub>AUC,PP</sub>	0.99	0.94	0.00	0.99	0.97	0.00
SUV <sub>AUC,WB</sub>	0.83	0.41	0.01	0.83	0.45	0.00
SUV <sub>PP</sub>	0.96	116.99	-0.46	0.92	129.57	-1.16
SUV <sub>WB</sub>	0.77	10.88	0.24	0.77	11.69	0.29
SUV <sub>BW</sub>	0.76	55.91	0.81	0.70	56.40	1.23
SUV <sub>LBM</sub>	0.73	41.64	0.75	0.70	40.97	1.06
SUV <sub>SHBG</sub>	0.80	2.88	-0.30	0.88	3.19	-0.03

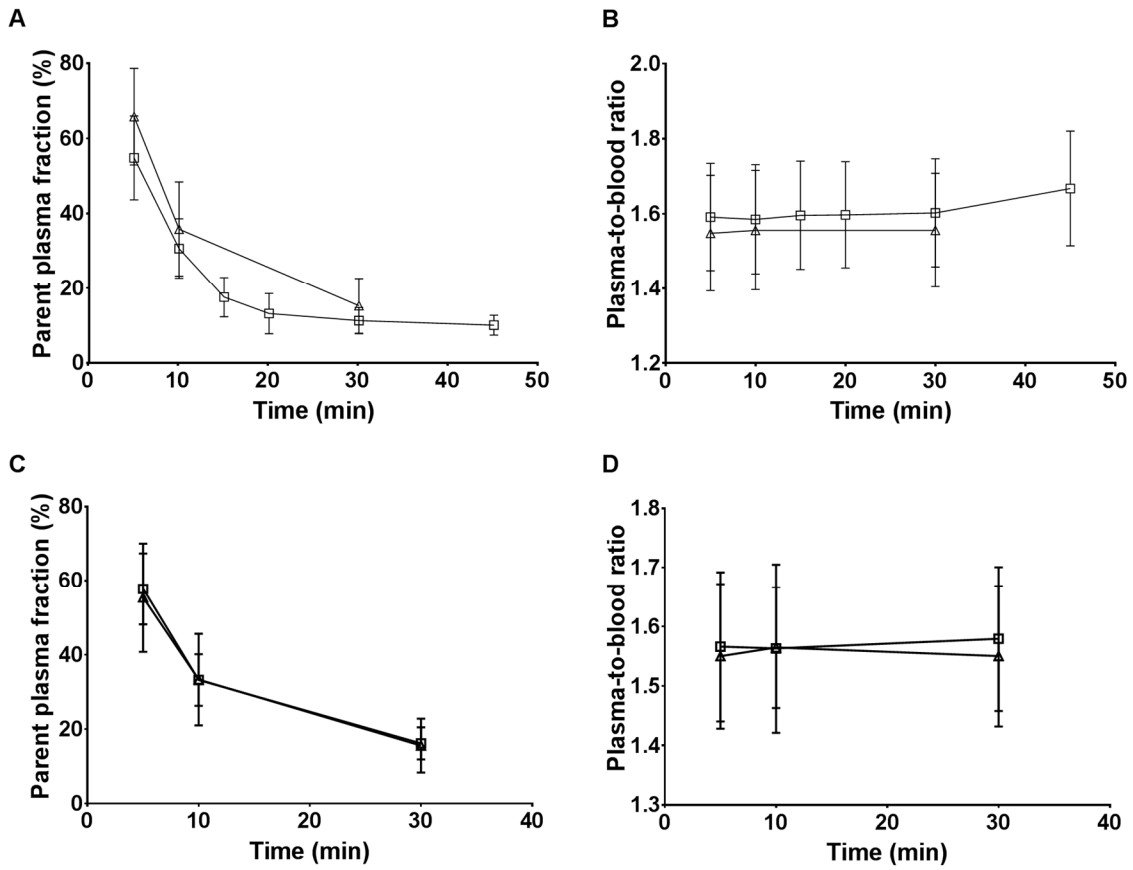
IDIF<sub>venous</sub>=Non-linear regression using image derived input function corrected using venous blood samples; SUV=Standardized uptake values; SUV<sub>AUC,PP</sub>=SUV normalized to the area under the parent plasma input curve; SUV<sub>AUC,WB</sub>=SUV normalized to the area under the whole blood input curve; SUV<sub>PP</sub>=SUV normalized to the parent plasma concentration; SUV<sub>WB</sub>=SUV normalized to the whole blood activity concentration; SUV<sub>BW</sub>=SUV normalized to bodyweight; SUV<sub>LBM</sub>=SUV normalized to lean body mass; SUV<sub>SHBG</sub>=SUV corrected for SHBG level.

Table 3: Repeatability coefficients of several quantitative <sup>18</sup>F-FDHT uptake metrics per lesion.

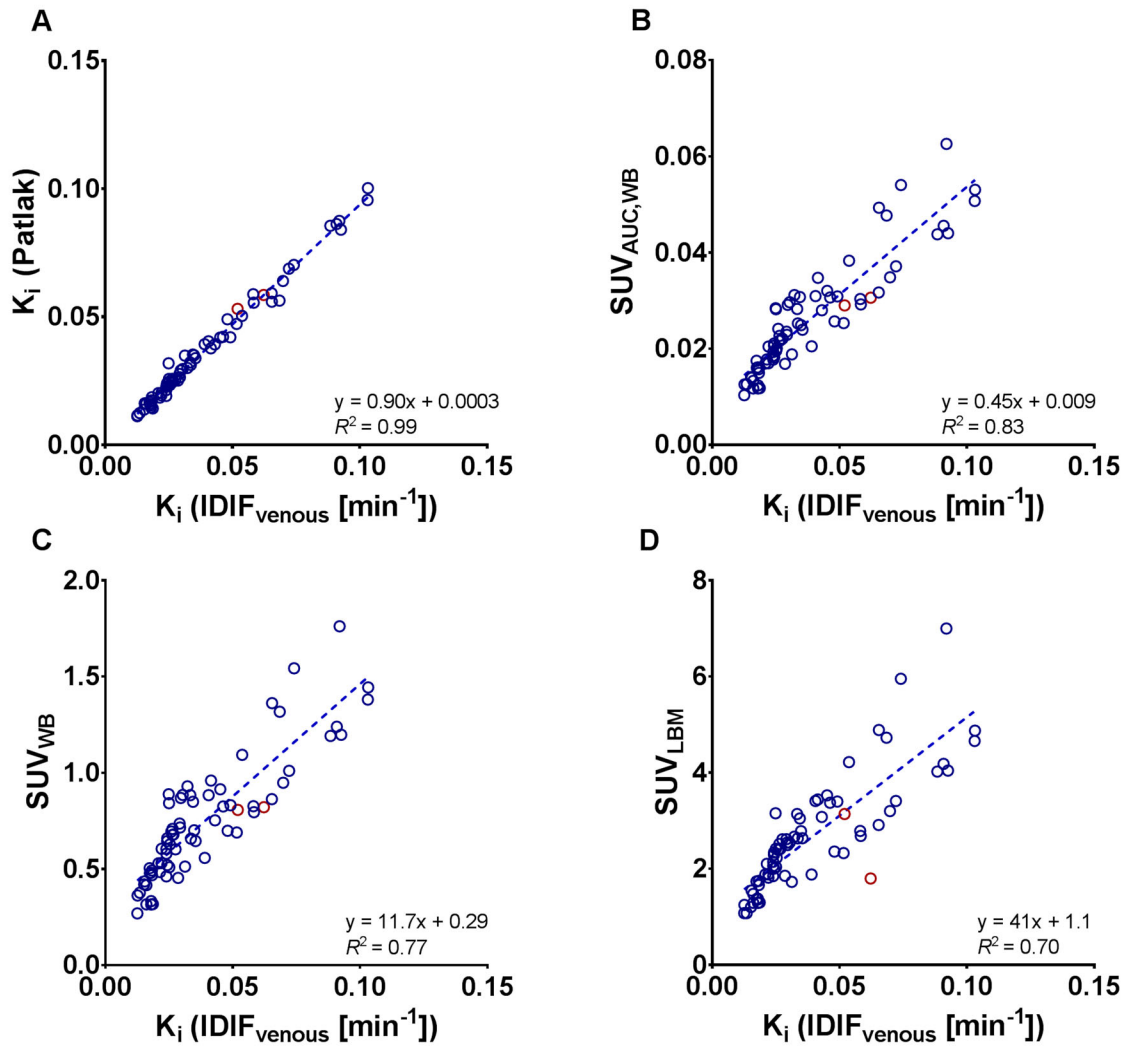
<i>Quantitative tracer uptake measures</i>	<i>Absolute difference</i>		<i>Relative difference</i>	
	<i>Mean</i>	<i>RC</i>	<i>Mean (%)</i>	<i>RC (%)</i>
IDIF <sub>venous</sub> K <sub>i</sub>	0.003	0.037	8.3	35.0
Patlak K <sub>i</sub>	0.003	0.034	8.2	31.3
SUV <sub>AUC,PP</sub>	0.003	0.038	7.4	25.1
SUV <sub>AUC,WB</sub>	0.002	0.023	3.1	23.7
SUV <sub>PP</sub>	0.089	4.178	11.4	55.8
SUV <sub>WB</sub>	0.062	0.660	2.4	25.1
SUV <sub>BW</sub>	0.277	2.878	4.2	27.1
SUV <sub>LBM</sub>	0.230	2.239	4.3	27.1

IDIF<sub>venous</sub>=Non-linear regression using image derived input function corrected using venous blood samples K<sub>i</sub>=Net influx rate; SUV=Standardized uptake values; SUV<sub>AUC,PP</sub>=SUV normalized to the area under the parent plasma input curve; SUV<sub>AUC,WB</sub>=SUV normalized to the area under the whole blood input curve; SUV<sub>PP</sub>=SUV normalized to the parent plasma concentration; SUV<sub>WB</sub>=SUV normalized to the whole blood activity concentration; SUV<sub>BW</sub>=SUV normalized to bodyweight; SUV<sub>LBM</sub>=SUV normalized to lean body mass

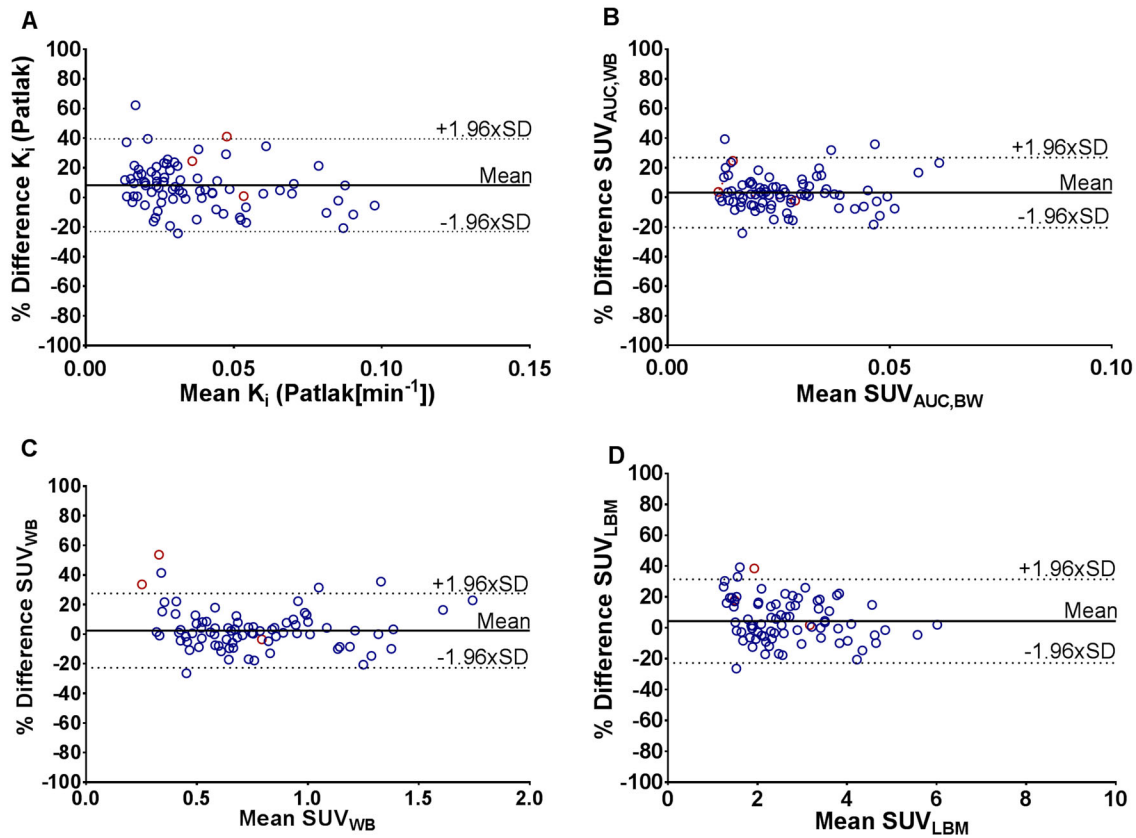
Supplemental materials:



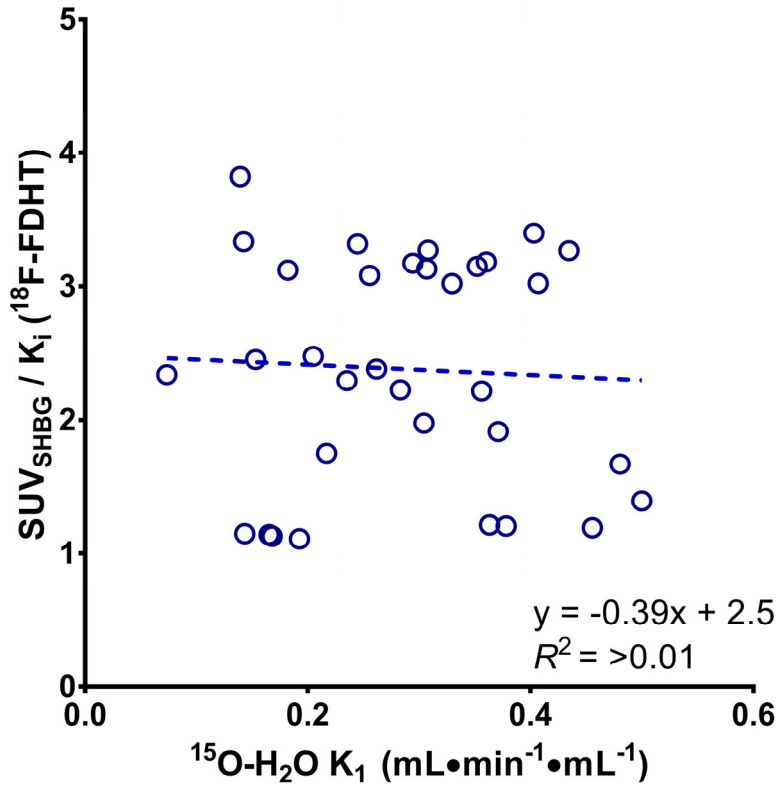
Supplemental figure 1:  $^{18}\text{F}$ -FDHT parent plasma fractions (A) and plasma-to-blood ratios (B) as function of time for arterial (squares) and venous (triangles) blood samples. Corresponding test-retest results for venous blood samples are shown in subplots C and D.



Supplemental figure 2: Scatterplots showing the correlation of  $^{18}\text{F}$ -FDHT Patlak based  $K_i$  (A),  $\text{SUV}_{\text{AUC,WB}}$  (B),  $\text{SUV}_{\text{WB}}$  (C) and  $\text{SUV}_{\text{LBM}}$  (D) with  $K_i$  obtained using an image derived input function corrected using venous blood samples.



Supplemental figure 3: Bland-Altman plots showing the relative differences in  $^{18}\text{F}$ -FDHT uptake between test and retest scans of Patlak (A),  $\text{SUV}_{\text{AUC,WB}}$  (B),  $\text{SUV}_{\text{WB}}$  (C) and  $\text{SUV}_{\text{LBM}}$  (D) plotted against the mean of test and retest uptake values.



Supplemental figure 4: Discrepancies between NLR based  $K_i$  using venous blood sampling and  $SUV_{BW}$  cannot be explained by differences in perfusion as assessed in this scatterplot using  $^{15}O-H_2O$  based  $K_1$ .

Supplemental table 1: Quantitative <sup>18</sup>F-FDHT uptake metrics

Continuous arterial sampling	Test		Retest	
	Median	IQR	Median	IQR
K <sub>1</sub>	0.12	0.05	-*	-*
K <sub>2</sub>	0.29	0.37	-*	-*
K <sub>3</sub>	0.21	0.15	-*	-*
V <sub>b</sub>	0.07	0.05	-*	-*
K <sub>i</sub>	0.05	0.04	-*	-*
<b>IDIF<sub>venous</sub></b>				
K <sub>1</sub>	0.11	0.09	0.11	0.06
K <sub>2</sub>	0.28	0.34	0.29	0.41
K <sub>3</sub>	0.15	0.10	0.16	0.17
V <sub>b</sub>	0.06	0.05	0.07	0.05
K <sub>i</sub>	0.03	0.03	0.03	0.03
<b>Simplified models</b>				
Patlak K <sub>i</sub>	0.03	0.03	0.03	0.02
SUV <sub>AUC,PP</sub>	0.03	0.03	0.04	0.03
SUV <sub>AUC,WB</sub>	0.02	0.01	0.02	0.02
SUV <sub>PP</sub>	2.27	3.08	3.20	2.54
SUV <sub>WB</sub>	0.69	0.38	0.69	0.48
SUV <sub>BW</sub>	3.05	1.78	3.06	2.10
SUV <sub>LBM</sub>	2.42	1.33	2.51	1.69
SUV <sub>SHBG</sub>	0.06	0.09	¥	¥

\* No arterial sampling was performed for the retest scans; ¥ SHBG levels were only determined prior to the first FDHT scan

IDIF<sub>venous</sub>=Non-linear regression using image derived input function corrected using venous blood samples; K<sub>i</sub>=Net influx rate; V<sub>b</sub>=Blood volume fraction; SUV=Standardized uptake values; SUV<sub>AUC,PP</sub>=SUV normalized to the area under the parent plasma input curve; SUV<sub>AUC,WB</sub>=SUV normalized to the area under the whole blood input curve; SUV<sub>PP</sub>=SUV normalized to the parent plasma concentration; SUV<sub>WB</sub>=SUV normalized to the whole blood activity concentration; SUV<sub>BW</sub>=SUV normalized to bodyweight; SUV<sub>LBM</sub>=SUV normalized to lean body mass; SUV<sub>SHBG</sub>=SUV corrected for SHBG level

Supplemental table 2: Repeatability coefficients of several quantitative <sup>18</sup>F-FDHT uptake metrics per lesion.

<i>Quantitative tracer uptake measures</i>	<i>Absolute difference</i>		<i>Relative difference</i>	
	<i>Mean</i>	<i>RC</i>	<i>Mean (%)</i>	<i>RC (%)</i>
IDIF <sub>venous</sub> K <sub>i</sub>	0.004	0.011	11.2	34.6
Patlak K <sub>i</sub>	0.003	0.009	10.1	28.3
SUV <sub>AUC,PP</sub>	0.003	0.010	10.0	20.9
SUV <sub>AUC,WB</sub>	0.003	0.007	2.4	15.0
SUV <sub>PP</sub>	0.002	2.253	10.1	61.3
SUV <sub>WB</sub>	0.054	0.196	6.6	19.7
SUV <sub>BW</sub>	0.184	0.732	6.5	23.8
SUV <sub>LBM</sub>	0.155	0.574	6.5	23.8

IDIF<sub>venous</sub>=Non-linear regression using image derived input function corrected using venous blood samples K<sub>i</sub>=Net influx rate; SUV=Standardized uptake values; SUV<sub>AUC,PP</sub>=SUV normalized to the area under the parent plasma input curve; SUV<sub>AUC,WB</sub>=SUV normalized to the area under the whole blood input curve; SUV<sub>PP</sub>=SUV normalized to the parent plasma concentration; SUV<sub>WB</sub>=SUV normalized to the whole blood activity concentration; SUV<sub>BW</sub>=SUV normalized to bodyweight; SUV<sub>LBM</sub>=SUV normalized to lean body mass